Inflationary gravitational waves and laboratory searches as complementary probes of right-handed neutrinos

Zafri A. Borboruah, 1,* Frank F. Deppisch, 2,† Anish Ghoshal, 3,‡ and Lekhika Malhotra, India Institute of Technology Bombay, Mumbai 400076, Maharashtra, India Department of Physics and Astronomy, University College London, Gower Street, London, WC1E 6BT, United Kingdom

Institute of Theoretical Physics, Faculty of Physics, University of Warsaw, ul. Pasteura 5, 02-093 Warsaw, Poland

(Received 12 June 2025; accepted 31 July 2025; published 2 September 2025)

We analyze the damping of inflationary gravitational waves (GW) that re-enter the Hubble horizon before or during a post inflationary era dominated by a metastable right-handed neutrino (RHN), whose out-of-equilibrium decay releases entropy. Within a minimal type-I seesaw extension of the Standard Model, we explore the conditions under which the population of thermally produced RHNs remain long-lived and cause a period of matter domination. We find that the suppression of the GW spectrum occurs above a characteristic frequency determined by the RHN mass and active-sterile mixing. For RHN masses in the range 0.1–10 GeV and mixing $10^{-12} \lesssim |V_{eN}|^2 \lesssim 10^{-5}$, we estimate such characteristic frequencies and the signal-to-noise ratio to assess the detection prospects in GW observatories such as THEIA, μ -ARES, LISA, BBO, and ET. Additionally we use LIGO data to put upper bounds on the reheating temperature after inflation, for a given blue-tilted GW spectrum. We find complementarity between GW signals and laboratory searches in SHiP, DUNE, and LEGEND-1000. Notably, RHN masses of 0.2–2 GeV and mixing $10^{-10} \lesssim |V_{eN}|^2 \lesssim 10^{-7}$ are testable in both laboratory experiments and GW observations. Additionally, GW experiments can probe the canonical seesaw regime of light neutrino mass generation, a region largely inaccessible to laboratory searches.

DOI: 10.1103/qyld-mf33

I. INTRODUCTION

All fermionic particles in the Standard Model (SM) of particle physics come in left- and right-handed variants except for the neutrinos, which are only left handed. This may be related to the fact that we observe neutrinos only through their left-handed SM interactions unlike the other particles. However, the SM fails to explain the masses of the neutrinos as evidenced by neutrino oscillation experiments [1–4]. The tiny neutrino masses $m_{\nu} \lesssim 0.1$ eV cannot be generated through the traditional Higgs mechanism since the Yukawa couplings between the left- and right-handed neutrinos required for generating sub-eV Dirac masses turn out to be of the order 10^{-12} , which is not

*Contact author: zafri123@iitb.ac.in †Contact author: f.deppisch@ucl.ac.uk; †Contact author: anish.ghoshal@fuw.edu.pl *Contact author: lekhika.malhotra@iitb.ac.in

Published by the American Physical Society under the terms of the Creative Commons Attribution 4.0 International license. Further distribution of this work must maintain attribution to the author(s) and the published article's title, journal citation, and DOI. Funded by SCOAP³. natural. Therefore, we might look into the possibility that neutrinos are of Majorana nature. The simplest way of Majorana neutrino mass generation is through the wellknown type-I seesaw mechanism [5–12], with heavy righthand neutrinos (RHNs). If the RHNs are sterile, i.e., uncharged under any gauge interactions, then the only coupling associated with them is through the Yukawa interaction with a left-handed lepton doublet and the Higgs doublet. If the heavy RHNs required by a viable type-I seesaw framework have masses in the MeV to TeV scale, they can be searched for in laboratory experiments, such as beta decays, meson decays, beam dump experiments, and colliders. For a comprehensive summary of such experiments, along with the existing constraints and future prospects of RHN searches, see, e.g., [13–15]. These RHN states are vastly heavier than the light active neutrinos, hence they are also referred to as heavy neutral leptons (HNLs).

The detection of gravitational waves (GWs) from black hole mergers by the LIGO and Virgo collaborations [16,17] and strong evidence for the presence of a stochastic GW background (SGWB) from measurements carried out by several pulsar timing array collaborations [18–24] have lead to postulations of beyond-the-Standard-Model (BSM)

new physics scenarios associated with GW production in the early Universe, including primordial origins of GWs related to cosmic inflation. Our work here proposes to form a synergy between GW observations and laboratory experiments involving seesaw and HNL searches. We will investigate quantum tensor fluctuations of the metric during cosmic inflation which propagate as gravitational waves in the post inflationary era. These GW modes go out of Hubble horizon during inflation [25–28]. Upon their horizon re-entry after inflation, these primordial gravitational waves (PGWs) can act as a book-keeping element of the cosmic expansion history of our Universe [29–37], since they propagate across all cosmological epochs and reach us today. Any deviation from the standard radiationdominated pre-BBN (big bang nucleosynthesis) history can be inferred by studying the features in the PGW spectral shapes since the expansion history of the Universe determines the redshifting of the GW amplitudes and frequencies to the present day [37–47]. In this regard, we consider an epoch where HNLs dominate the energy budget of the Universe, thus affecting its post inflationary evolution, which leads to characteristic GW spectral shapes testable in various current and upcoming GW detectors. Such primordial features in the GW spectrum usually reveal two important quantities: (a) the time when HNL matter domination began, which is set by the highest frequency that departs from a flat spectrum, and (b) the duration of HNL matter domination, which corresponds to the width of the feature in frequency space [45,47–55].

Long-lived HNLs are notoriously difficult to detect in conventional collider experiments due to their displaced vertices, which render them effectively invisible [56]. For HNLs with masses in the range 0.1 GeV \lesssim 10 GeV, beam dump, long-lived particle search experiments, such as deep underground neutrino experiment (DUNE) [57,58], MAssive Timing Hodoscope for Ultra-Stable neutraL pArticles (MATHUSLA) [59,60], and search for hidden particles (SHiP) [61] offer promising prospects for probing large regions of the parameter space. Nevertheless, even if an HNL is detected, the information extracted is typically limited to its mass and lifetime, leaving the rest of the hidden sector poorly constrained. It is therefore of significant importance to find complementary sources of information about such long-lived HNLs. We propose, in this paper, that primordial features in the SGWB from the inflationary paradigm will be useful in obtaining independent evidence for and information on HNLs. This suggests a potential synergy between GW observatories and laboratory experiments in testing such a BSM scenario.

The paper is organized as follows: In Sec. II, we give a review of type-I seesaw and HNL decays along with current and future HNL searches. In Sec. III, we discuss the conditions for HNL domination in the early Universe and Sec. IV covers the suppression of primordial gravitational waves of inflationary origin due to HNL domination and we show the future projections of deviations in signal-to-noise

ratio of the suppressed GW spectra due to HNL domination as compared to the standard spectra for various GW experiments. We demonstrate the complementarity of GW searches with laboratory searches in the HNL parameter space. Finally, in Sec. V, we conclude and discuss future implications.

II. HEAVY NEUTRAL LEPTONS

As the underlying model, we consider the conventional type-I seesaw with three HNLs N_i ,

$$\mathcal{L} = \sum_{\alpha i} y_{\alpha i} \overline{L_{\alpha}} (i\sigma_2) H^{\dagger} N_i + \frac{1}{2} \sum_{i} m_{N_i} \overline{N_i^c} N_i + \text{h.c..}$$
 (1)

Here, L_{α} are the SM lepton doublets ($\alpha = e, \mu, \tau$), H is the SM Higgs doublet and σ_2 is the second Pauli matrix. We assume, without loss of generality that the symmetric RHN mass matrix is diagonal, $M_N = \text{diag}(m_{N_1}, m_{N_2}, m_{N_3})$. After electroweak symmetry breaking with $\langle H \rangle \equiv v \sim 174$ GeV, the light active neutrinos acquire and effective Majorana mass matrix $M_{\nu} = -m_D \cdot M_N^{-1} \cdot m_D^T$, at leading order in the seesaw expansion with $m_D \equiv yv \ll M_N$. It is diagonalized by the PMNS mixing matrix U_{PMNS} , constrained by measurements of neutrino oscillations. The RHN Majorana mass term is a priori unconstrained, as it is unrelated to SM electroweak symmetry breaking; it can in principle have any scale from eV and below to the Planck scale. We here consider HNLs with masses in the range 0.1 GeV $\leq m_N \leq$ 10 GeV as the regime of interest for direct searches and motivated by viable low-scale leptogenesis.

In the following, we work in a simplified scenario with a single HNL denoted by N. We ignore any flavor structure and we assume that the HNL dominantly couples to the electron-flavor active neutrino and the Lagrangian (1) simplifies to

$$\mathcal{L} = y_{eN} \overline{L_e} (i\sigma_2) H^{\dagger} N + \frac{1}{2} m_N \overline{N^c} N + \text{H.c.}$$
 (2)

A light active neutrino mass scale $m_{\nu} = |V_{eN}|^2 m_N$ is then generated, where V_{eN} is the admixture between the active neutrino and the HNL, $V_{eN} = y_{eN} v/m_N$. We treat m_N and $|V_{eN}|^2$ as free parameters. The focus of our paper is to study the interplay between the constraints and future sensitivity reaches from laboratory HNL searches and GW detectors. We do not attempt to consider the full light neutrino mass spectrum and the PMNS mixing pattern observed in oscillations. Instead, we take the limit on the effective β decay mass, $m_{\beta} < 0.45$ eV at 90% confidence level (CL), from KATRIN [62] as an upper limit on m_{ν} , whereas solar neutrino oscillations point toward a smallest scale $m_{\nu} > \sqrt{\Delta m_{\rm sol}^2} \approx 9 \times 10^{-3}$ eV [63]. Thus, successful neutrino mass generation favors a parameter space of interest 9×10^{-3} eV $< |V_{eN}|^2 m_N < 0.45$.

For GeV-scale HNLs, this requires very small activesterile mixing strengths,

$$|V_{eN}|^2 = \frac{m_{\nu}}{m_N} \lesssim 10^{-10} \left(\frac{1 \text{ GeV}}{m_N}\right),$$
 (3)

resulting in long-lived HNLs that can be searched through their displaced vertices in laboratory experiments. On the other hand, if such long-lived HNLs are present in the early Universe, they can trigger a period of intermediate matter domination that can imprint on the GW spectrum arising due to tensor perturbations generated during cosmic inflation. We should emphasize, though, that the relation in Eq. (3) is not strictly required. Smaller mixing is possible if there are other contributions to the light neutrino masses, such as from additional HNLs. Likewise, the mixing can be larger if lepton number is approximately conserved. This is not only achieved in the limits $m_N \to 0$ and $m_N \to \infty$ but also if pairs of HNLs form Dirac fermion states themselves. By feebly violating lepton number symmetry, e.g., through a Majorana mass term $\mu \ll m_N$, light neutrino masses are generated, $|m_{\nu}| \sim (y_{\nu} v/m_N)^2 \mu = |V_{\ell N}|^2 \mu$, while the HNLs form quasi-Dirac pairs with a small mass splitting $\Delta m_N \sim \mu$.

A. HNL decays and direct searches

This section summarizes the most relevant HNL decay channels, considering both charged and neutral current interactions as mediators. Most results for sufficiently light HNLs are already established in the literature [13–15] and we use the partial decay widths summarized in [64]. Two basic processes contribute to the decay modes: charged current decays leading to final particles such as lepton pairs (ν_e, e) or up/down quark pairs (u, d), and neutral current decays, leading to fermion pairs $f\bar{f}$. For the decays $N \to \nu_e e^-e^+$ and $N \to \nu_e \nu_e \bar{\nu}_e$, both processes can contribute, with interference. The general formula for charged current-mediated processes, such as $N \to e^-\nu_\beta \mathcal{E}_\beta^+$ $(\beta \neq e)$ and $N \to e u_i \bar{d}_i$, is

$$\Gamma(N \to e^- u \bar{d}) = \frac{G_F^2 m_N^5}{192 \pi^3} |V_{eN}|^2 I(x_u, x_d, x_e), \qquad (4)$$

where $G_F=1.166\times 10^{-5}~{\rm GeV^{-2}}$ is the Fermi constant and $x_e=\frac{m_e}{m_N},\,x_u=\frac{m_u}{m_N},\,x_d=\frac{m_d}{m_N}$. The function $I(x_u,x_d,x_l)$ accounts for corrections due to finite masses of the final-state fermions. The full expression is given in [13,65]. Likewise, the decay width for neutral current-mediated decays $N\to \nu_e f\bar{f}$ depends on the types of final fermions. For the case of pure neutrino final states, the decay width simplifies to

$$\Gamma(N \to \nu_e \nu_{\beta} \bar{\nu}_{\beta}) = (1 + \delta_{e\beta}) \frac{G_F^2 m_N^5}{768 \pi^3} |V_{eN}|^2.$$
 (5)

At masses below the QCD scale ($m_N \lesssim \Lambda_{\rm QCD}$), the decay products form single mesons, and decay modes involving

charged and neutral mesons are considered. The decay widths for these processes are derived for charged pseudoscalar mesons (π^0, η) , charged vector mesons (ρ^\pm, a_1^\pm) , and neutral vector mesons (ρ^0, a_1^0) . For HNLs with masses above 1 GeV, multihadron final states become kinematically accessible. The total hadronic decay width, $\Gamma_{\rm had}$, is estimated by comparing the decay width into quarks and the corresponding loop corrections, which are similar to those found for τ -lepton decays. QCD corrections are expected to be less than 30% for HNLs with $m_N \gtrsim 1$ GeV. Overall, the full hadronic decay width dominates for $m_N \gtrsim 1$ GeV.

Corresponding to their total decay width, HNLs are naturally long-lived if light compared to the mediating SM gauge bosons and for the small active-sterile mixing strength expected for successful light neutrino mass generation,

$$L_N \approx 25 \text{ mm} \cdot \frac{10^{-10}}{|V_{\ell N}|^2} \cdot \left(\frac{10 \text{ GeV}}{m_N}\right)^2.$$
 (6)

This approximation is roughly valid for 1 GeV $\lesssim m_N \lesssim m_W$. HNLs lighter than a few GeV can be abundantly produced in beam dump experiments through meson decays, resulting in displaced vertex signatures that can be searched for with small background rates. As representative examples, we will highlight the sensitivity of DUNE [57,58], MATHUSLA [59,60], and SHiP [61], to compare with GW observations in the framework considered here. The strong sensitivity of such high-luminosity, displaced-vertex searches will be shown in Figs. 4 (right) and 6, which shows the future sensitivities as well as current constraints on the active-sterile mixing strength $|V_{eN}|^2$ as function of the HNL mass m_N .

B. Neutrinoless double beta decay

The most sensitive probe of the Majorana nature of light active neutrinos is $0\nu\beta\beta$ decay [66]. In addition, $0\nu\beta\beta$ decay is sensitive to other exotic sources of lepton number violation [67–74]. This includes the exchange of Majorana HNLs. In the simplified scenario of a single HNL mixing with electron flavor, the decay half-life $T_{1/2}^{0\nu}$ for $m_N \gtrsim 100$ MeV is approximately [75]

$$\frac{10^{28} \text{ yr}}{T_{1/2}^{0\nu}} \approx \left(\frac{|V_{eN}|^2}{10^{-9}} \cdot \frac{1 \text{ GeV}}{m_N}\right)^2.$$
 (7)

Here, nuclear matrix elements for the isotope 76 Ge [70] are used. The dependence is modified around the $0\nu\beta\beta$ momentum scale ≈ 100 MeV and at the crossover, the momentum dependence should be accounted for more carefully [76,77]. The sensitivity in Eq. (7) is compared with $T_{1/2}^{0\nu}(^{76}\text{Ge}) = 10^{28}$ yr, the projected reach of large enriched germanium experiment for neutrinoless

double-beta decay (LEGEND)-1000 [78]. Current experimental limits are of the order $T_{1/2}^{0\nu} \gtrsim 10^{26}$ yr [79,80]. In Figs. 4 (right) and 6, we likewise show the sensitivity of $0\nu\beta\beta$ decay searches to HNLs, in comparison with direct searches and GW observations.

III. HNL DOMINATION IN THE EARLY UNIVERSE

As discussed above, the HNL can interact with the SM plasma due to the active-sterile mixing via scattering, annihilation, and decays. At temperatures much higher than m_N , the interaction rate is approximated as $\Gamma_N^{\text{int}} \sim G_F^2 T^5 |V_{eN}|^2$. The HNL will be thermally produced if the following condition is satisfied [81–85],

$$\Gamma_N^{\text{int}}(T_{\text{max}}) > 3\mathcal{H}(T_{\text{max}}),$$
 (8)

where $\mathcal{H}(T) = \sqrt{\frac{8\pi^3 g_\star(T)}{90}} \frac{T^2}{M_{\mathrm{Pl}}}$ is the Hubble rate during radiation domination with g_* being the relativistic degrees of freedom and $M_{\mathrm{Pl}} = 1.22 \times 10^{19}$ GeV being the Planck mass. The factor 3 is usually taken in cosmology because in an expanding Universe, the interaction rates should be significantly larger than the Hubble rate in order to bring the interacting species to thermal equilibrium. T_{max} is the temperature when N production is maximum, given by [83,86,87]

$$T_{\text{max}} \sim 10 \text{ GeV} \left(\frac{m_N}{1 \text{ GeV}}\right)^{1/3}$$
. (9)

This is derived by considering temperature and momentum-dependent mixing strength of the HNL below electroweak scale [84,88]. In this paper, we are only interested in thermally produced HNLs. This gives a lower bound on the mixing strength above which N can enter thermal equilibrium [83],

$$|V_{eN}|^2 \gtrsim 6 \times 10^{-12} \left(\frac{1 \text{ GeV}}{m_N}\right).$$
 (10)

After production, N remains in equilibrium until its interaction with SM plasma freezes out at temperature T_f . The evolution of the energy densities of N and radiation at temperatures below T_f are estimated by the following set of coupled Boltzmann equations,

$$\dot{\rho}_{N} = -3\mathcal{H}(\rho_{N} + p_{N}) - \langle \Gamma_{N} \rangle (\rho_{N} - \rho_{N}^{eq}),$$

$$\dot{\rho}_{R} = -4\mathcal{H}\rho_{R} + \langle \Gamma_{N} \rangle (\rho_{N} - \rho_{N}^{eq}),$$
(11)

where $\langle \Gamma_N \rangle$ is the thermally averaged total decay width of N. We ignored the scattering and annihilation terms because they are frozen out below T_f . The dot denotes differentiation with respect to cosmic time. Here ρ_N and $\rho_N^{\rm eq}$ denote the energy density and equilibrium energy density of N, respectively, while ρ_R corresponds to the radiation energy density of the Universe. The term p_N represents the

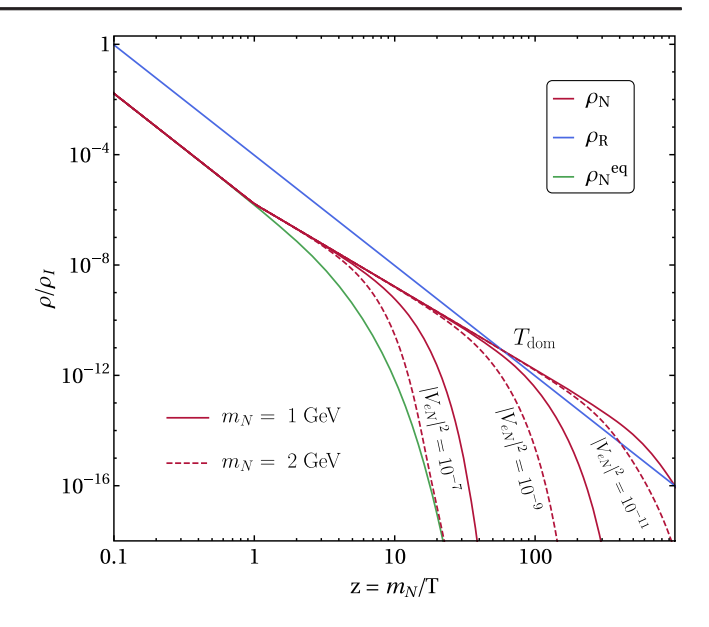


FIG. 1. HNL energy density evolution, obtained by solving the Boltzmann Eq. (11), for varying m_N and $|V_{eN}|^2$ as depicted (red solid and dashed curves). For comparison, the green curve represents the HNL equilibrium energy density whereas the blue curve shows the radiation energy density. $T_{\rm dom}$ indicates the temperature of intermediate HNL matter domination with mass $m_N=1~{\rm GeV}$ as an example.

pressure of the HNL gas. To account for the transition between relativistic (radiationlike) and nonrelativistic (matterlike) regimes of N evolution, we assume $p_N = \rho_N/3$ for $T \gtrsim m_N$ and $p_N = 0$ for $T \lesssim m_N$, where T is the temperature of the Universe.

In Fig. 1, we show the solutions of the Boltzmann equations. The blue solid line illustrates the evolution of the radiation energy density as a function of the parameter $z=m_N/T$. The red lines depict the evolution of the energy density of N, while the green solid line represents the equilibrium energy density. The values of m_N and $|V_{eN}|^2$ are given within the plot. For z<1, N behaves as radiation, and its energy density evolves as a^{-4} . For z>1, N becomes nonrelativistic and its energy density evolves as matter ($\propto a^{-3}$). We consider a thermal abundance of N at z=0.1 [which means Eq. (10) is satisfied] and demonstrate the effect of m_N and $|V_{eN}|^2$ on the evolution.

As shown in the plot, increasing the value of $|V_{eN}|^2$ leads to an earlier decay of N. Before decaying, N becomes nonrelativistic as long as its total decay width is smaller than the Hubble rate at temperatures around m_N , i.e., $\Gamma_N \ll \mathcal{H}(m_N)$. Assuming that the decay is instantaneous and the decay products thermalize with the radiation bath quickly, the decay temperature $T_{\rm dec}$ can be estimated from the condition $\Gamma_N \sim \mathcal{H}(T_{\rm dec})$ as

$$T_{\rm dec} \sim \left(\frac{90}{8\pi^3 g_*(T_{\rm dec})}\right)^{\frac{1}{4}} \sqrt{\Gamma_N M_{\rm Pl}}.$$
 (12)

For sufficiently small values of m_N and $|V_{eN}|^2$, the energy density of N eventually overtakes the radiation energy density at temperature $T_{\rm dom}$ as shown in the plot for $|V_{eN}|^2=10^{-11}$, giving rise to an early matter-dominated epoch. For an initial thermal abundance of N, one can calculate $T_{\rm dom}$ as [48,89]

$$T_{\text{dom}} \sim \frac{7}{4} \frac{m_N}{q_*(T_{\text{dom}})} \sim 2\% \, m_N.$$
 (13)

We require $T_{\rm dec} < T_{\rm dom}$ for the existence of the HNL-dominated epoch. The decay of the nonrelativistic dominating HNL species into SM particles ends the matter domination, injecting entropy into the Universe and diluting all energy densities. The effect of this dilution is seen as suppression of inflationary gravitational waves as we will discuss in the next section. Figure 2 shows the timeline of key events.

The effect on GW spectrum depends on the dilution factor \mathcal{D} , which is the ratio of comoving entropy density after and before the decay event. Assuming the decay products of N thermalize quickly with the radiation bath, the dilution factor at the end of the N-dominated epoch can be approximated as [48,49,90],

$$\mathcal{D} = \frac{s(T_{\text{after}})a^{3}(T_{\text{after}})}{s(T_{\text{before}})a^{3}(T_{\text{before}})}$$

$$= \left(1 + 2.95 \left(\frac{2\pi^{2}\langle g_{*}(T)\rangle}{45}\right)^{\frac{1}{3}} \frac{\binom{n_{N}}{s}m_{N})^{\frac{4}{3}}}{(M_{\text{Pl}}\Gamma_{N})^{\frac{2}{3}}}\right)^{\frac{3}{4}}, \quad (14)$$

where s and a are the entropy density and the scale factor, respectively. $T_{\rm before/after}$ represents the temperature just before/after the decay. The initial abundance of N is given as the ratio n_N/s . We assume that N freezes out while still being relativistic in the parameter range considered. Hence the maximum value of N abundance is [91],

$$\frac{n_N}{s} = \frac{135\zeta(3)}{4\pi^4 q_{*S}},\tag{15}$$

where g_{*S} is the number of relativistic degrees of freedom contributing to entropy density and we consider it to be ~ 106.75 for our analysis. We will use this dilution factor as well as the decay temperature to calculate the GW spectra later.

IV. PRIMORDIAL GRAVITATIONAL WAVES

The early Universe underwent an exponential expansion phase known as inflation. This phase was followed by the reheating process, which generated a high-energy plasma consistent with the Standard Model of particle physics. During inflation, PGWs emerged as quantum tensor fluctuations in the metric. Initially, while outside the cosmological horizon, these GWs maintained constant amplitudes. However, once the GWs re-entered the horizon during the radiation-dominated epoch, their amplitudes experienced damping. The propagation of GW modes that re-enter the horizon is characterized by a transfer function. We follow Refs. [48–51] to present the standard GW spectrum and then introduce a new concept of relative SNR to disentangle signals of EMD.

A. Gravitational waves spectrum

The energy density spectrum of the GWs, denoted as $\Omega_{\rm GW}(k)$, depends on the wave number $k=2\pi f$, where f is the frequency of the GWs [48]. It is given as

$$\Omega_{\text{GW}}(k) = \frac{1}{12} \left(\frac{k}{a_0 H_0}\right)^2 T_T^2(k) P_T^{\text{prim}}(k),$$
(16)

where $a_0 = 1$ is the present-day scale factor, and $H_0 \approx 2.2 \times 10^{-4} \; \mathrm{Mpc^{-1}}$ represents the current Hubble expansion rate [52]. Here, $P_T^{\mathrm{prim}}(k)$ is the primordial tensor power spectrum, and $T_T^2(k)$ is the transfer function describing the evolution of GWs as they propagate through a Friedmann-Lemaitre-Robertson-Walker background. The horizon reentry temperature T_{in} is expressed as [39],

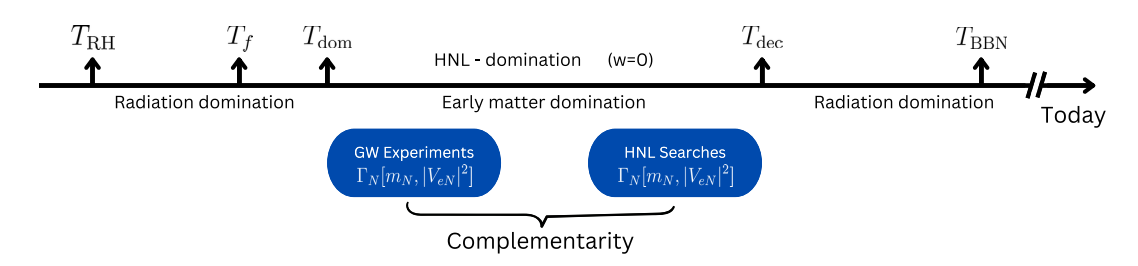


FIG. 2. Schematic timeline of key events and eras of cosmic evolution. After reheating ends at $T_{\rm RH}$, HNLs are produced thermally from the SM plasma. The interactions decouple and HNLs freeze-out at temperature T_f . Eventually, HNLs become nonrelativistic at temperatures comparable to the HNL mass, $T \approx m_N$. At $T_{\rm dom}$, HNLs start to dominate the energy density of the Universe. This gives rise to a period of matter domination until the HNLs decay at around $T_{\rm dec}$, kick-starting a second radiation dominated epoch before BBN. The modified expansion of the Universe during the HNL-dominated era suppresses the GW spectrum from inflation, depending on m_N and the active-sterile mixing $|V_{eN}|^2$. This effect can be detected in future GW experiments, complementing HNL laboratory searches.

$$T_{\rm in} = 5.8 \times 10^6 \text{ GeV} \left(\frac{106.75}{g_*(T_{\rm in})}\right)^{1/6} \left(\frac{k}{10^{14} \text{ Mpc}^{-1}}\right), \quad (17)$$

where $g_*(T_{\rm in})$ is the effective number of relativistic degrees of freedom at temperature $T_{\rm in}$.

The primordial tensor power spectrum $P_T^{\text{prim}}(k)$ can be parametrized in terms of its amplitude A_T and spectral index n_T , defined at the pivot scale $k_* = 0.05 \text{ Mpc}^{-1}$ [92],

$$P_T^{\text{prim}}(k) = A_T(k_*) \left(\frac{k}{k_*}\right)^{n_T}.$$
 (18)

The amplitude $A_T(k_*)$ is related to the scalar power spectrum $A_S(k_*)$ and the tensor-to-scalar ratio r, with an upper bound $r \le 0.035$ from BICEP/Keck observations [93],

$$A_T(k_*) = A_S(k_*)r, \quad A_S(k_*) = 2.0989 \times 10^{-9}.$$
 (19)

For our analysis, we fix r = 0.035. In standard single-field slow-roll inflation with Bunch-Davies initial vacuum, the spectral index n_T satisfies the consistency relation $n_T \approx -r/8$ [94], leading to a red-tilted spectrum ($n_T < 0$). However, alternative inflationary models and particle production models allow for deviations, including a blue-tilted spectrum ($n_T > 0$), which have significant theoretical motivation and have been thoroughly analyzed in the literature [95–102]. For our purpose we will keep n_T as a free parameter.

The transfer function $T_T^2(k)$ is determined analytically and numerically as

$$T_T^2(k) = \Omega_m^2 \left(\frac{g_*(T_{\rm in})}{g_*^0}\right) \left(\frac{g_{*S}^0}{g_{*S}(T_{\rm in})}\right)^{4/3} \left(\frac{3j_1(z_k)}{z_k}\right)^2 F(k), \tag{20}$$

where $g_*^0 = 3.36$ and $g_{*S}^0 = 3.91$ are the present-day values of the relativistic degrees of freedom. The total matter density parameter is $\Omega_m = 0.31$ [52]. Here, $j_1(z_k)$ is the spherical Bessel function, with $z_k \equiv k\tau_0$ and $\tau_0 = 2/H_0$. For $z_k \gg 1$, corresponding to the frequencies of interest, the damping factor simplifies to $j_1(z_k) \sim 1/(\sqrt{2}z_k)$. The fitting function F(k) varies depending on the thermal history of the Universe.

In standard cosmology, the fitting function F(k) is given by [103]

$$F(k)_{\text{standard}} = T_1^2 \left(\frac{k}{k_{\text{eq}}}\right) T_2^2 \left(\frac{k}{k_{\text{RH}}}\right), \tag{21}$$

whereas in the presence of an intermediate matter domination (IMD) phase, it takes the form

$$F(k)_{\text{IMD}} = T_1^2 \left(\frac{k}{k_{\text{eq}}}\right) T_2^2 \left(\frac{k}{k_{\text{dec}}}\right) T_3^2 \left(\frac{k}{k_{\text{dec S}}}\right) T_2^2 \left(\frac{k}{k_{\text{RH S}}}\right). \tag{22}$$

The key scales appearing above are given by,

$$k_{\rm eq.} = 7.1 \times 10^{-2} \,\mathrm{Mpc^{-1} \cdot \Omega_m h^2},$$
 (23)

$$k_{\text{dec}} = 1.7 \times 10^{14} \text{ Mpc}^{-1} \left(\frac{g_{*S}(T_{\text{dec}})}{g_{*S}^0} \right)^{1/6} \left(\frac{T_{\text{dec}}}{10^7 \text{ GeV}} \right),$$
(24)

$$k_{\rm RH} = 1.7 \times 10^{14} \text{ Mpc}^{-1} \left(\frac{g_{*S}(T_{\rm RH})}{g_{*S}^0}\right)^{1/6} \left(\frac{T_{\rm RH}}{10^7 \text{ GeV}}\right),$$
(25)

$$k_{\text{dec S}} = k_{\text{dec}} \mathcal{D}^{2/3}, \quad k_{\text{RH S}} = k_{\text{RH}} \mathcal{D}^{-1/3}.$$
 (26)

Here, $T_{\rm dec}$ [defined in Eq. (12)] and $T_{\rm RH}$ correspond to the reheating temperatures from HNL and inflaton decay, respectively, with h=0.7 being the reduced Hubble parameter. The factor $\mathcal D$ accounts for the entropy dilution during the IMD phase, defined in Eq. (14).

The fit functions $T_1^2(x)$, $T_2^2(x)$, and $T_3^2(x)$ are defined as

$$T_1^2(x) = 1 + 1.57x + 3.42x^2,$$

$$T_2^2(x) = (1 - 0.22x^{3/2} + 0.65x^2)^{-1},$$

$$T_3^2(x) = 1 + 0.59x + 0.65x^2.$$
 (27)

Using Eq. (16), the GW spectrum $\Omega_{\rm GW}h^2$ as a function of the current frequency can be plotted. The spectrum undergoes suppression above a characteristic frequency $f_{\rm sup}$, given by [29]

$$f_{\text{sup}} \simeq 2.7 \times 10^{-8} \text{ Hz} \left(\frac{T_{\text{dec}}}{\text{GeV}}\right).$$
 (28)

The suppression factor, R_{sup} , comparing the IMD spectrum to the standard case, reads

$$R_{\text{sup}} = \frac{\Omega_{\text{GW}}^{\text{IMD}}}{\Omega_{\text{GW}}^{\text{standard}}} \simeq \frac{1}{\mathcal{D}^{4/3}}.$$
 (29)

Ideally when $\mathcal{D}=1$, there is no suppression and $\Omega_{\rm GW}^{\rm IMD}$ approximates $\Omega_{\rm GW}^{\rm standard}$. However, the numerical formulas in Eq. (27), especially the 0.59x factor in $T_3^2(x)$ produces a bump in the GW spectrum for small values of the dilution factor \mathcal{D} (see Fig. 1 in [32]). As suggested therein, we ignore this 0.59x factor for $\mathcal{D} \leq 10$, but we still see a small bump when $\mathcal{D} < 2$. Therefore, we take a smooth interpolation from $\Omega_{\rm GW}^{\rm IMD}$ to $\Omega_{\rm GW}^{\rm standard}$ as \mathcal{D} varies from 10 to 1,

$$\Omega_{\rm GW}^{\rm interpolation} = \Omega_{\rm GW}^{\rm IMD} + (\Omega_{\rm GW}^{\rm standard} - \Omega_{\rm GW}^{\rm IMD}) \left[\frac{2}{1 + e^{-p(\mathcal{D})}} - 1 \right], \tag{30}$$

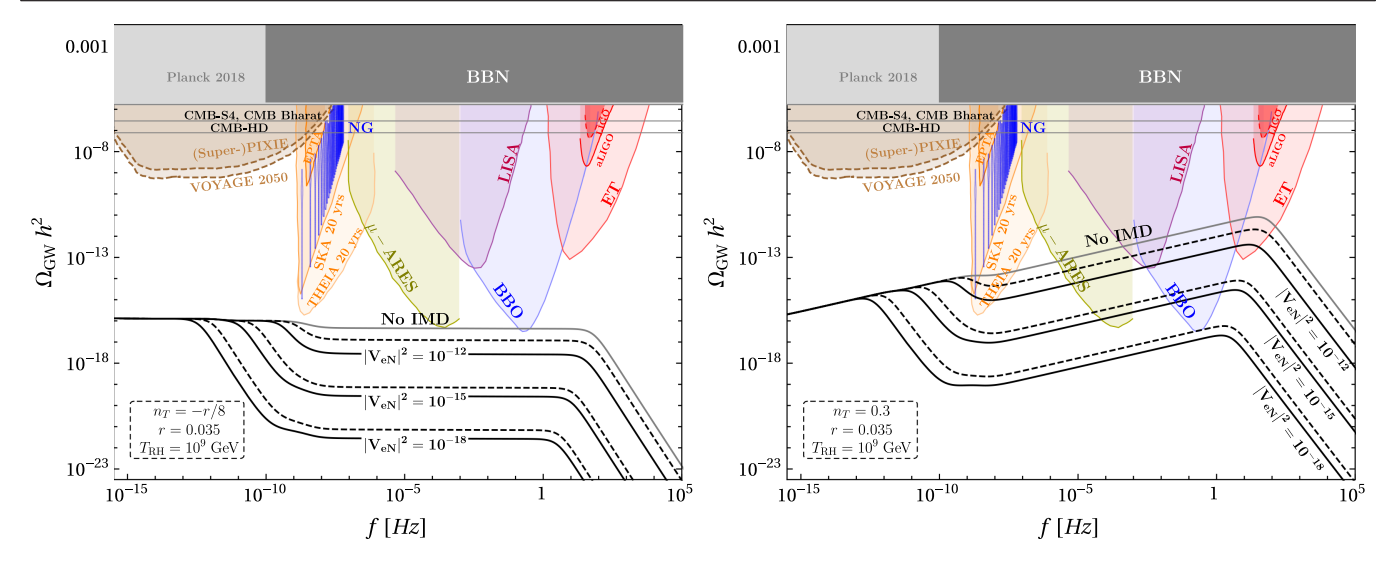


FIG. 3. Example GW spectra demonstrating the effect of varying the HNL mass m_N and the active-sterile mixing $|V_{eN}|^2$ on suppression depicted by the black solid ($m_N=3$ GeV) and dashed ($m_N=5$ GeV) curves. Left and right plots correspond to spectral indices $n_T=-r/8$ (implying slow-roll inflation) and 0.3 (blue tilted), respectively. The gray solid curve indicates the case without HNLs and thus no intermediate matter domination. Other parameters we have taken are r=0.035, $T_{\rm RH}=10^9$ GeV. The dark/light gray regions on top are the current $\Delta N_{\rm eff}$ bounds from BBN and cosmic microwave background (CMB), respectively, that rule out $\Omega_{\rm GW}h^2\gtrsim 10^{-6}$. The red region corresponding to LIGO is also ruled out. The other colored regions represent expected sensitivities of future GW observations.

where $p(\mathcal{D})$ depends on the dilution. For p=0, the spectrum is described by $\Omega_{\rm GW}^{\rm IMD}$ while for large p values, the spectrum smoothly transitions to $\Omega_{\rm GW}^{\rm standard}$. We take the form of the parameter $p(\mathcal{D})=10e^{-(\mathcal{D}-1)}$ for our analysis.

In Fig. 3, we show example GW spectra for various values of m_N and $|V_{eN}|^2$. The left plot shows the spectra for $n_T = -r/8$ corresponding to slow-roll inflation, with r = 0.035. The right plot shows blue-tilted spectra with $n_T = 0.3$. The standard PGW spectrum is represented by the solid gray curve, corresponding to no intermediate matter domination. The dashed and solid black curves are the suppressed spectra for $m_N = 5$ and 3 GeV, respectively. We take $T_{\rm RH} = 10^9$ GeV for both the plots and demonstrate the effects of n_T , m_N , and $|V_{eN}|^2$ on the suppression of the spectra.

The shaded colored regions represent the noise curves for various existing and upcoming gravitational wave experiments, including LIGO [16,17], aLIGO [104], big bang observer (BBO) [105], laser interferometer space antenna (LISA) [106], einstein telescope (ET) [107], THEIA [108], μ ARES [109], European pulsar timing array [110], and square kilometer array (SKA) [20]. The blue violin curves show recent NANOGrav (NG) results [23]. Future missions such as Super-PIXIE [111] and VOYAGE 2050 [112] are designed to detect gravitational wave signals through spectral distortions in the cosmic microwave background. The current bounds on $\Delta N_{\rm eff}$ from BBN and CMB are shown as gray boxes at the top while the future projections are shown as horizontal gray lines.

In Fig. 4, the left panel shows the GW spectra for the benchmark points given in Table I, while the right panel

shows the benchmark points in the HNL parameter space. The purple dashed, blue dot-dashed, red dotted, and green-dotted lines show the damped GW spectra with HNL domination for the benchmark points BP1, BP2, BP3, and BP4. The shaded region indicates the GW sensitivity curves of the SKA and THEIA experiments. In the right panel, colored dashed lines represent the projected sensitivities of DUNE, MATHUSLA, and SHiP, while the dotdashed black line shows the BBN bound on the lifetime of HNL [81]. Below the BBN line, the lifetime of HNL exceeds ~ 0.02 s and for m_N larger than the mass of pion, the decay of HNL to pions during BBN can lead to overproduction of primordial helium-4. Hence this region must be excluded. The gray region at the bottom represents nonthermal production of HNL where Eq. (10) is not satisfied and we have not studied that region in this paper. BP1 lies within the sensitivity of SHiP and LEGEND-1000, while BP2 and BP3 fall within DUNE's, indicating potential signals in both GW and laboratory experiments. Note that BP3 is excluded by BBN, however this is a weak bound due to inherent uncertainties in its calculation. Recent studies [113,114] provide more stringent constraints on the parameter space m_N vs $|V_{eN}|^2$ by analyzing the effects of matter-domination during BBN in light of CMB and BBN data. Future experiments such as CMB-S4 are expected to provide significantly improved measurements, potentially tightening these constraints further.

B. Signal-to-noise ratio

Interferometers serve as precision instruments to measure displacements caused by gravitational waves (GWs),

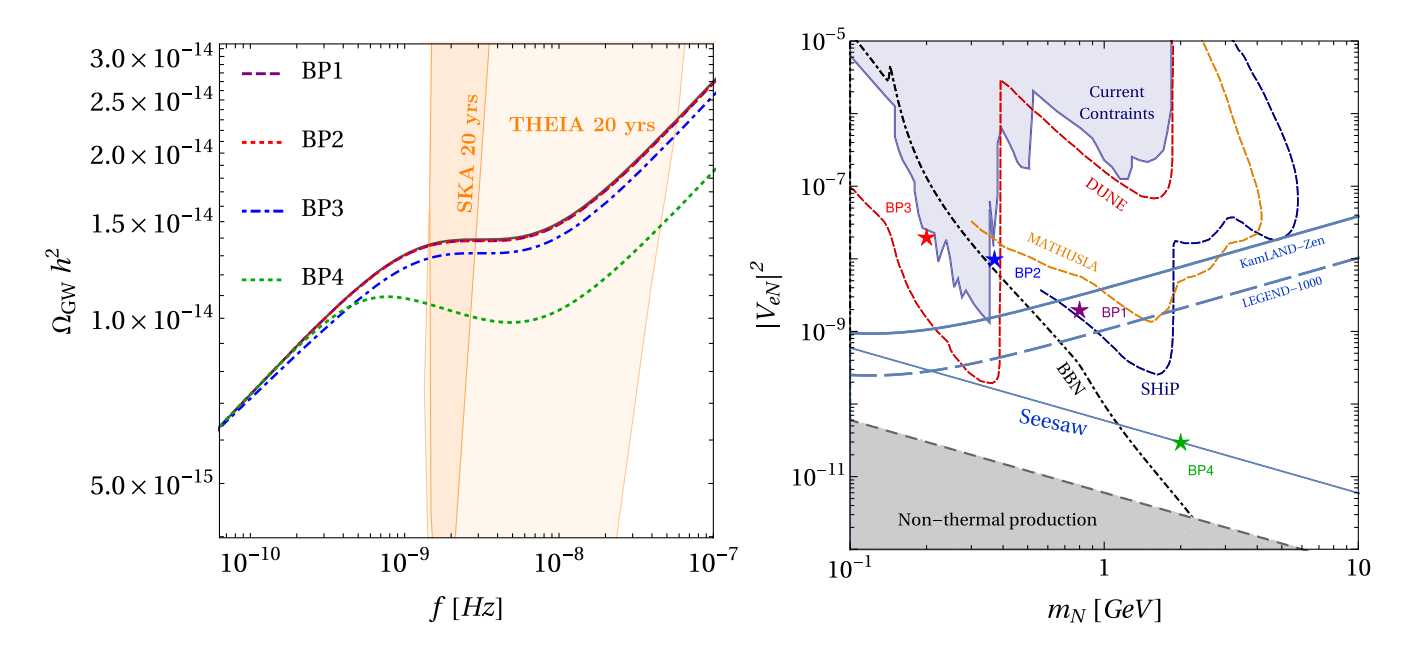


FIG. 4. Left: GW spectra for the benchmark points in Table I, with the primordial tensor spectral index $n_T=0.3$ and the tensor-to-scalar ratio r=0.035. The colored regions represent the sensitivity of the future GW observations at SKA and THEIA. Right: Current constraints (blue region) and future sensitivities (colored curves labeled DUNE, MATHUSLA, SHiP) of direct HNL searches on the active-sterile mixing $|V_{eN}|^2$ as a function of the HNL mass m_N . Also shown are the current constraint from $0\nu\beta\beta$ decay at KamLAND-Zen and the future $0\nu\beta\beta$ decay sensitivity at LEGEND-1000. The region to the left of the curve labeled "BBN" is disfavored by big bang nucleosynthesis and HNLs are not thermally produced in the gray region. The line labeled "Seesaw" indicates successful neutrino mass generation, $m_{\nu} = |V_{eN}|^2 m_N = 0.1$ eV, in the canonical seesaw. The stars indicate the same benchmark points from Table I as in the left panel.

expressed in terms of the dimensionless strain-noise $h_{\rm GW}(f)$. The strain noise is intrinsically connected to the amplitude of gravitational waves and can be translated into the corresponding energy density spectrum. This relationship is given by

$$\Omega_{\rm exp}(f)h^2 = \frac{2\pi^2 f^2}{3H_0^2} h_{\rm GW}^2(f)h^2, \tag{31}$$

where H_0 is the present-day Hubble expansion rate, defined as $H_0 = h \times 100 \frac{\text{km/s}}{\text{Mpc}}$, with h denoting the dimensionless Hubble parameter.

To determine the detectability of the primordial gravitational wave background, we compute the signal-to-noise

ratio (SNR) based on the experimental sensitivity curve $\Omega_{\exp}(f)h^2$, which may represent current measurements or future projections. The SNR is given by

$$SNR \equiv \sqrt{\tau \int_{f_{min}}^{f_{max}} df \left(\frac{\Omega_{GW}(f)h^2}{\Omega_{exp}(f)h^2}\right)^2},$$
 (32)

where τ is the total observation time and the integral runs over the frequency range $[f_{\min}, f_{\max}]$. For the purposes of this analysis, we assume an observation time of $\tau = 4$ yrs and set h = 0.7. A detection threshold is established by requiring a signal-to-noise ratio of SNR ≥ 10 [115,116]. In Fig. 5, we show regions with SNR > 10 in the parameter

TABLE I. Benchmark points and their SNR_{rel} projections in THEIA, μ -ARES, LISA, BBO, and ET. BP1 comes within sensitivity of SHiP and LEGEND-1000, while BP2 and BP3 are sensitive in DUNE. The benchmark BP4 satisfies the type-I seesaw relation and generates light neutrino masses. The value of tensor-to-scalar ratio is r = 0.035 and inflationary reheating temperature is $T_{\rm RH} = 10^9$ GeV.

			$\mathrm{SNR}_{\mathrm{rel}} \times 100\%$				
			$n_T = -r/8$		$n_T = 0.3$		
Benchmark	m_N (GeV)	$ V_{eN} ^2$	BBO	μ-ARES	THEIA	LISA	ET
BP1	0.80	2×10^{-9}	0.8%	0.8%	0.5%	0.8%	0.8%
BP2	0.37	1×10^{-8}	0.5%	0.5%	0.4%	0.5%	0.5%
BP3	0.20	2×10^{-8}	5.8%	5.8%	5.5%	5.8%	5.8%
BP4	2.00	3×10^{-11}	31.7%	31.7%	22.4%	31.7%	31.7%

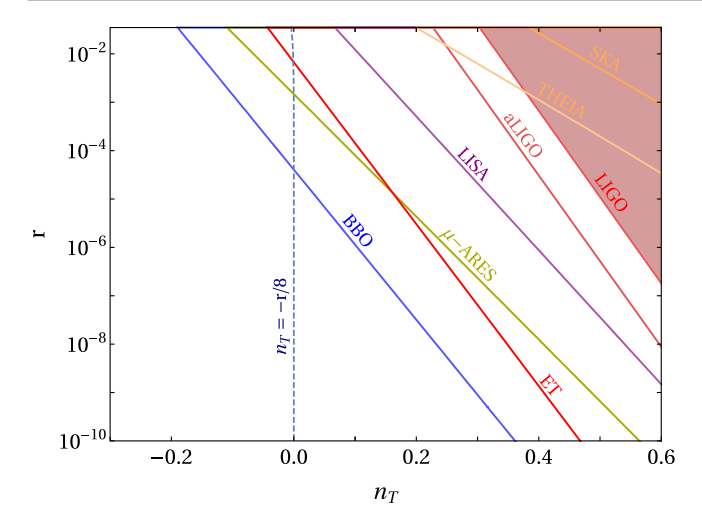


FIG. 5. Future detectability of standard PGW spectra (no intermediate matter domination) across GW experiments. Regions to the right of each colored line indicate where SNR > 10 in the (n_T, r) parameter space for different GW experiments. The dashed line $n_T \approx -r/8$ denotes standard slow-roll inflation. We fix $T_{\rm RH} = 10^9$ GeV.

space spanned by n_T and r for different future GW experiments. Here, we only consider the standard primordial GW spectra and assume a reheating temperature of $T_{\rm RH}=10^9$ GeV. The vertical dashed line corresponding to $n_T\approx -r/8$ represents the standard slow-roll inflation, which can be tested only with BBO, ET, and μ -ARES. We see that $n_T>0$ is required to get a detectable GW signal in LISA, THEIA, and SKA. The figure illustrates that primordial GWs are in principle detectable over a wide range of parameters. While positive values of n_T are preferred, this includes predictions from standard slow-roll inflation. Such a signal is then further modified by the IMD driven by a right-handed neutrino species in the early universe as our main effect of interest.

C. Bounds from dark radiation

We present here the effective constraints on dark radiation arising due to BBN and CMB decoupling. Since gravitons behave as massless radiationlike degrees of freedom, the primordial gravitational wave (GW) energy density considered should remain below the observational limits on any such additional dark radiation. This is conventionally expressed in terms of deviations in the effective number of relativistic degrees of freedom, $\Delta N_{\rm eff}$. The constraint on $\Omega_{\rm GW}(f)$ at the time of recombination is usually expressed in terms of [117]

$$\int_{f_{\min}}^{\infty} \frac{\mathrm{d}f}{f} \Omega_{\text{GW}}(f) h^2 \le 5.6 \times 10^{-6} \Delta N_{\text{eff}}.$$
 (33)

Here, the lower bound of integration, $f_{\rm min}$, typically differs depending on the cosmological epoch under consideration. Particularly, we know that for BBN, $f_{\rm min} \sim 10^{-10}$ Hz, while

for CMB constraints, it is approximately taken to be $f_{\rm min} \sim 10^{-18}$ Hz. Nonetheless, as for all practical purposes, such as when comparing multiple GW spectra or analyzing their peak contributions, it is more than sufficient to approximate these constraints by ignoring the detailed frequency dependence and instead focusing only on the total energy density at the spectral peak. This simplifies a lot and consequently leads to the expression

$$\Omega_{\rm GW}^{\rm Peak} h^2 \le 5.6 \times 10^{-6} \Delta N_{\rm eff}. \tag{34}$$

For our present analysis, we incorporate current bounds on $\Delta N_{\rm eff}$ derived from BBN observations and the PLANCK 2018 data from Ref. [118]. Additionally, we explore the sensitivity reach of upcoming CMB experiments, including CMB-S4 [119,120], CMB-Bharat [121], and CMB-HD [122,123]. These we expect to significantly refine the constraints on $\Delta N_{\rm eff}$ or discover extra dark radiation and, consequently, provide sensitivity reaches on the primordial GW energy density.

D. Results

We present the projected sensitivities of future GW experiments in the parameter space of the HNL. In Fig. 6, we show laboratory searches for HNL described in Sec. II, along with contours of the relative SNR defined as

$$SNR_{rel} \equiv \frac{SNR_{std} - SNR_{IMD}}{SNR_{std}}$$
 (35)

for various GW experiments where SNR_{std} is the SNR of the standard spectra, which is a constant for a given GW experiment given fixed values of r, n_T and T_{RH} . SNR_{IMD} is the SNR of the suppressed GW spectra due to HNL domination. The quantity SNR_{rel} signifies the deviation of the GW spectra from the expected standard spectra such that larger value of SNR_{rel} correspond to larger suppression. It varies between 0 and 1 with 0 signifying no suppression and 1 signifying huge suppression or no detection prospect. Another benefit of showing SNR_{rel} instead of just showing SNR_{IMD} is that the effects of r, n_T , and T_{RH} are canceled out in SNR_{rel}. For μ -ARES and BBO, we take $n_T = -r/8$ corresponding to slow-roll inflation, with r = 0.035. However, for THEIA, LISA, and ET, we take $n_T = 0.3$. We find that for $n_T = 0.3$, all the benchmark points are ruled out by LIGO data if $T_{\rm RH} \gtrsim 10^9$ GeV. We take $T_{\rm RH} =$ 10⁹ GeV for all the plots in Fig. 6. The light brown region signifies the scenario where HNLs do not dominate in the early Universe, hence $SNR_{rel} \sim 0$ (due to numerical uncertainties, we ignore $SNR_{rel} < 0.003$), i.e., we can not differentiate the GW spectra from the standard spectra. The yellow region is where $0.003 \le \Delta SNR \le 0.9$ while the red region is where $SNR_{rel} > 0.9$. We put a threshold, SNR > 10 for these plots signifying a 5σ detection prospect at all these GW experiments. The white region in the bottom left of each plot

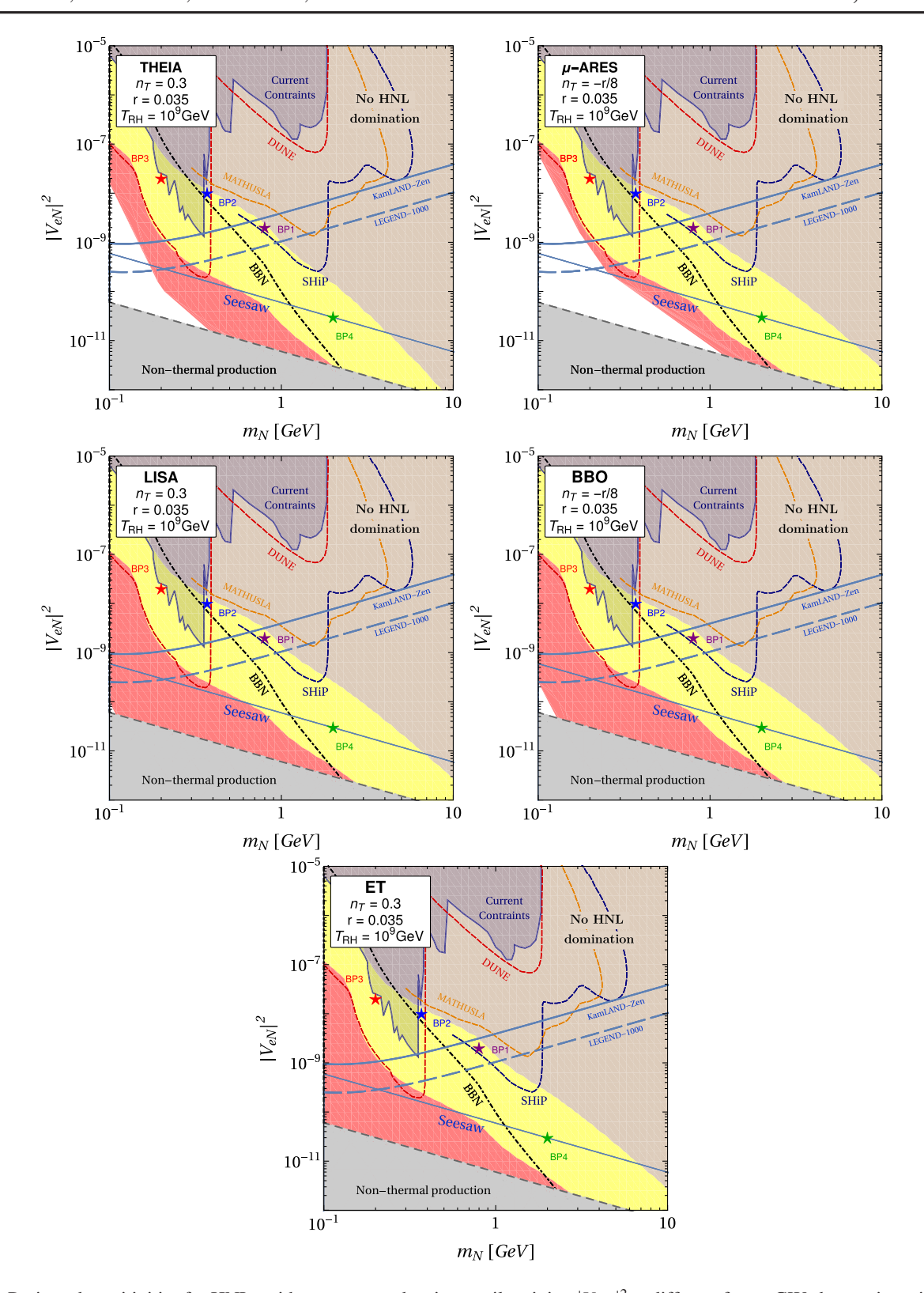


FIG. 6. Projected sensitivities for HNLs with mass m_N and active-sterile mixing $|V_{eN}|^2$ at different future GW observations, in terms of the relative signal-to-noise ratio $\text{SNR}_{\text{rel}} < 0.003$ (no HNL domination, brown region); $0.003 \leq \text{SNR}_{\text{rel}} \leq 0.9$ (weak domination, yellow region); $\text{SNR}_{\text{rel}} \geq 0.9$ (strong domination, red region). A white region in the bottom left indicates an absolute $\text{SNR}_{\text{IMD}} < 10$ that is undetectable in the given GW observation. For comparison, each panel shows the current constraints and future sensitivities from direct and $0\nu\beta\beta$ decay searches for HNLs, as described in Fig. 4.

represents $SNR_{IMD} < 10$, i.e., GW is difficult to detect in this region due to large suppression.

The value of n_T taken for each plot is shown in the plot. The four benchmark points BP1, BP2, BP3, and BP4 are testable in both GW and laboratory experiments. The corresponding values of SNR_{rel} for the benchmark points at various GW experiments are shown in Table I. We find that $SNR_{rel} < 1\%$ in case of BP1 and BP2 in all GW experiments, implying marginal complementarity of GW experiments with SHiP and DUNE. However we see there

is a region in the parameter space (0.6 GeV $\lesssim m_N \lesssim 1$ GeV and $|V_{eN}| \sim 10^{-9}$) with large SNR_{rel}, which is also sensitive to LEGEND-1000. GW searches can also probe regions of the parameter space where no laboratory searches reach. For example GW can probe the seesaw line (solid blue line) where active neutrino masses are successfully generated via the seesaw mechanism, as depicted by the benchmark BP4. Note that for all the benchmark points, SNR_{rel} in THEIA is smaller than that in other experiments. This is due to the fact that for all the benchmark points, the frequency of

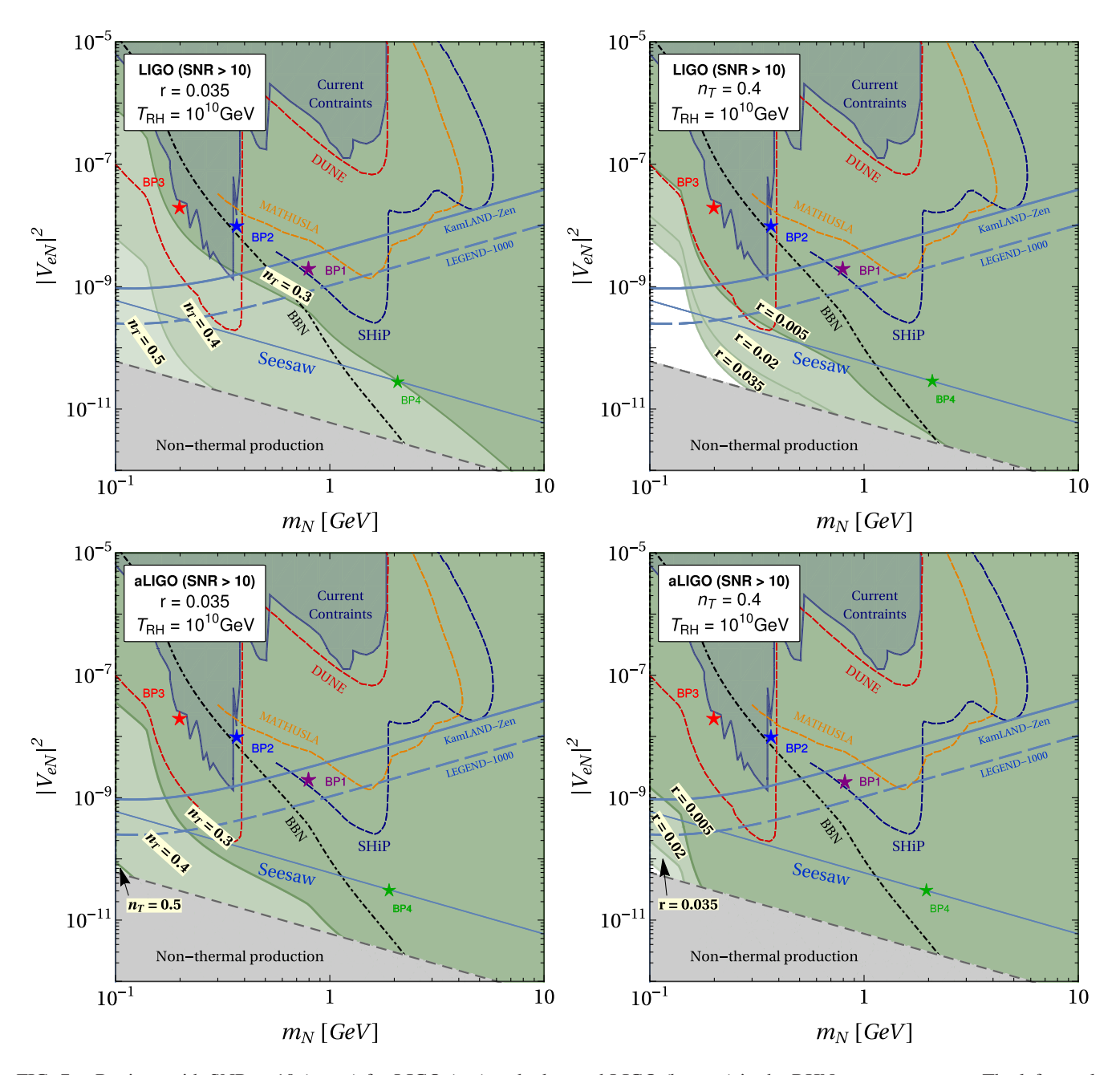


FIG. 7. Regions with SNR > 10 (green) for LIGO (top) and advanced LIGO (bottom) in the RHN parameter space. The left panels show the effect of varying the spectral index, $n_T = 0.3$, 0.4, and 0.5, keeping the tensor-to-scalar ratio r = 0.035. The right panels show the effect of varying r = 0.035, 0.02, and 0.005, for a fixed value of $n_T = 0.4$. All plots assume a constant reheating temperature $T_{\rm RH} = 10^{10}$ GeV.

suppression f_{sup} defined in Eq. (28) lies within the frequency range of THEIA.

E. Constraints from LIGO

LIGO is a large-scale experiment designed to detect high-frequency gravitational waves in the range of approximately 30-207 Hz. Its upgraded version, aLIGO, features significantly enhanced sensitivity over a broader frequency band, extending from ~20 to 450 Hz. Data from aLIGO's fourth observational run is expected to be released by the end of 2025. Figure 7 shows the current and projected constraints from LIGO and aLIGO in the parameter space of m_N and $|V_{eN}|^2$. The green shaded regions in the upper panels show SNR > 10 constraints for LIGO, while the lower panels display projected regions for aLIGO. The left column explores variations in the tensor spectral index n_T for fixed r, whereas the right column varies r at fixed n_T . In all plots, the reheating temperature $T_{RH} = 10^{10} \text{ GeV}$ is assumed. It can be clearly seen that higher value of n_T and rincreases the amplitude of GW hence increasing SNR in the LIGO and aLIGO. We find that for $n_T = 0.3$ and $T_{\rm RH} \le 10^9$ GeV, LIGO does not put any constraint on the considered parameter space. Hence, the HNL parameter space is allowed in Fig. 6 for $T_{RH} = 10^9$ GeV.

V. DISCUSSION AND CONCLUSIONS

Inflationary gravitational waves offer us a unique window into heavy and high energy particle physics that is otherwise inaccessible to terrestrial experiments [45,124–129]. In this work, we show that GWs can probe long-lived RHNs by discerning deviations from the standard thermal history due to a brief period of early matter domination during the pre-BBN era. Starting from a thermal initial abundance, the suppressed decay rate of RHNs enables them to survive and dominate the energy budget of the universe temporarily, leaving imprints in the inflationary GW spectrum in the form of a characteristic dip in the amplitude. The entire setup is therefore described by a minimal set of independent parameters: the mass of RHNs, m_N , and the active-sterile mixing, $|V_{eN}|^2$. We find a novel complementary signature for longlived RHNs in GW searches THEIA, LISA, ET, μ-ARES, and BBO, by studying the effect on the GW spectral shape caused by a period of early matter domination due to longlived RHN, see Fig. 3. We find that ET, THEIA, and LISA will not be able to detect significant suppression of PGW spectra for $n_T \lesssim -r/8$ with r = 0.035. Specifically, THEIA and LISA require $n_T \gtrsim 0.3$ for detection. However, in this case, LIGO rules out most of the parameter space considered, if $T_{\rm RH} \gtrsim 10^9$ GeV. In Fig. 5 we show the regions with SNR > 10 for standard GW spectra without IMD in the parameter space (n_T, r) . We find that very small parameter space gives a detectable signal for experiments like BBO, ET, and μ -ARES under the standard slow roll scenario. For other GW experiments such as LISA, THEIA, and ET, a blue-tilted PGW spectrum ($n_T > 0$) will be detectable.

We compare the resulting sensitivity with that of laboratory searches for RHNs, namely beam dump experiments and $0\nu\beta\beta$ decay, where long-lived RHNs can be searched for experimentally in light-dark sector searches involving intensity, lifetime, and beam dump experiments. We explored the parameter space in Fig. 6, highlighting the projected sensitivity of long-lived particle searches at DUNE, MATHUSLA, and SHiP as well as the $0\nu\beta\beta$ decay search at LEGEND-1000. Interestingly, we demonstrated overlapping regions of sensitivity in such searches with detectable signals within four years of exposure for the GW detectors considered. These may serve as complementary signatures for RHNs and give a deep insight into the mechanism of neutrino mass generation. This is expected to enhance the existing complementarity between laboratory searches [130] and would provide direct evidence of RHNs in early cosmology. The RHN mass and mixing range probed by laboratory experiments and GW detectors is 0.2 GeV $\lesssim m_N \lesssim 2$ GeV and $10^{-10} \lesssim |V_{eN}|^2 \lesssim 10^{-7}$, as evident from Fig. 4.

In addition, GW detectors can probe regions of parameter space not reachable by laboratory experiments, particularly the canonical seesaw regime of light neutrino mass generation. This regime is difficult to probe with direct laboratory and GW signals may not only be able to shed light on this important seesaw regime but also various well-motivated dark sectors, especially in the weakly coupled regimes, such as the neutrino-portal portal freeze-in dark matter [65], axionportal RHNs [131], and low scale leptogenesis [132]. We plan to look into such analyses in a future publication. We emphasize again that hunting for apparently disjointed signals in laboratory experiments and cosmological probes will help us to break degeneracies beyond the SM theories of cosmology that involve multiple energy scales and heavy scales, thus providing a possible pathway to the community and a promising way to search for new physics in the upcoming years.

ACKNOWLEDGMENTS

Z. A. B. is supported by the IoE fund at IIT Bombay. L. M. is supported by an UGC scholarship. F. F. D. acknowledges support from the UK Science and Technology Facilities Council (STFC) via the Consolidated Grant No. ST/X000613. A. G. thanks Stefan Pokorski and Deep Ghosh for discussions.

DATA AVAILABILITY

The data are not publicly available. The data are available from the authors upon reasonable request.

- [1] R. Davis, A review of the Homestake solar neutrino experiment, Prog. Part. Nucl. Phys. **32**, 13 (1994).
- [2] Y. Fukuda *et al.* (Super-Kamiokande Collaboration), Evidence for oscillation of atmospheric neutrinos, Phys. Rev. Lett. **81**, 1562 (1998).
- [3] K. Eguchi *et al.* (KamLAND Collaboration), First results from KamLAND: Evidence for reactor anti-neutrino disappearance, Phys. Rev. Lett. **90**, 021802 (2003).
- [4] Q. R. Ahmad *et al.* (SNO Collaboration), Direct evidence for neutrino flavor transformation from neutral current interactions in the Sudbury Neutrino Observatory, Phys. Rev. Lett. **89**, 011301 (2002).
- [5] P. Minkowski, $\mu \rightarrow e\gamma$ at a rate of one out of 10^9 muon decays?, Phys. Lett. **67B**, 421 (1977).
- [6] R. N. Mohapatra and G. Senjanovic, Neutrino mass and spontaneous parity nonconservation, Phys. Rev. Lett. 44, 912 (1980).
- [7] M. Gell-Mann, P. Ramond, and R. Slansky, Complex spinors and unified theories, Conf. Proc. C 790927, 315 (1979), https://inspirehep.net/literature/9686.
- [8] T. Yanagida, Horizontal gauge symmetry and masses of neutrinos, Conf. Proc. C 7902131, 95 (1979), https:// inspirehep.net/literature/143150.
- [9] S. L. Glashow, The future of elementary particle physics, NATO Sci. Ser. B **61**, 687 (1980).
- [10] J. Schechter and J. W. F. Valle, Neutrino masses in $SU(2) \times U(1)$ theories, Phys. Rev. D **22**, 2227 (1980).
- [11] T. Yanagida, Horizontal symmetry and masses of neutrinos, Prog. Theor. Phys. 64, 1103 (1980).
- [12] R. N. Mohapatra and G. Senjanović, Neutrino mass and spontaneous parity nonconservation, Phys. Rev. Lett. **44**, 912 (1980).
- [13] A. Atre, T. Han, S. Pascoli, and B. Zhang, The search for heavy Majorana neutrinos, J. High Energy Phys. 05 (2009) 030
- [14] P. D. Bolton, F. F. Deppisch, and P. S. Bhupal Dev, Neutrinoless double beta decay versus other probes of heavy sterile neutrinos, J. High Energy Phys. 03 (2020) 170.
- [15] A. M. Abdullahi *et al.*, The present and future status of heavy neutral leptons, J. Phys. G **50**, 020501 (2023).
- [16] B. P. Abbott *et al.* (LIGO Scientific and Virgo Collaborations), Observation of gravitational waves from a binary black hole merger, Phys. Rev. Lett. **116**, 061102 (2016).
- [17] B. P. Abbott *et al.* (LIGO Scientific and Virgo Collaborations), GW151226: Observation of gravitational waves from a 22-solar-mass binary black hole coalescence, Phys. Rev. Lett. 116, 241103 (2016).
- [18] C. L. Carilli and S. Rawlings, Science with the square kilometer array: Motivation, key science projects, standards and assumptions, New Astron. Rev. 48, 979 (2004).
- [19] G. Janssen *et al.*, Gravitational wave astronomy with the SKA, Proc. Sci. AASKA14 (**2015**) 037 [arXiv:1501.00127].
- [20] A. Weltman *et al.*, Fundamental physics with the Square Kilometre Array, Pub. Astron. Soc. Aust. **37**, e002 (2020).
- [21] L. Lentati *et al.* (EPTA Collaboration), European pulsar timing array limits on an isotropic stochastic gravitational-wave background, Mon. Not. R. Astron. Soc. **453**, 2576 (2015).

- [22] S. Babak *et al.* (EPTA Collaboration), European pulsar timing array limits on continuous gravitational waves from individual supermassive black hole binaries, Mon. Not. R. Astron. Soc. 455, 1665 (2016).
- [23] G. Agazie *et al.* (NANOGrav Collaboration), The NANO-Grav 15 yr data set: Evidence for a gravitational-wave background, Astrophys. J. Lett. **951**, L8 (2023).
- [24] A. Afzal *et al.* (NANOGrav Collaboration), The NANOGrav 15 yr data set: Search for signals from new physics, Astrophys. J. Lett. **951**, L11 (2023); Astrophys. J. Lett. **971**, L27(E) (2024).
- [25] L. P. Grishchuk, Amplification of gravitational waves in an istropic universe, Zh. Eksp. Teor. Fiz. **67**, 825 (1974), http://www.jetp.ras.ru/cgi-bin/dn/e_040_03_0409.pdf.
- [26] A. A. Starobinsky, Spectrum of relict gravitational radiation and the early state of the universe, JETP Lett. 30, 682 (1979), https://inspirehep.net/literature/147727.
- [27] V. A. Rubakov, M. V. Sazhin, and A. V. Veryaskin, Graviton creation in the inflationary universe and the grand unification scale, Phys. Lett. **115B**, 189 (1982).
- [28] M. C. Guzzetti, N. Bartolo, M. Liguori, and S. Matarrese, Gravitational waves from inflation, Riv. Nuovo Cimento 39, 399 (2016).
- [29] N. Seto and J. Yokoyama, Probing the equation of state of the early universe with a space laser interferometer, J. Phys. Soc. Jpn. **72**, 3082 (2003).
- [30] L. A. Boyle and P. J. Steinhardt, Probing the early universe with inflationary gravitational waves, Phys. Rev. D 77, 063504 (2008).
- [31] L. A. Boyle and A. Buonanno, Relating gravitational wave constraints from primordial nucleosynthesis, pulsar timing, laser interferometers, and the CMB: Implications for the early Universe, Phys. Rev. D **78**, 043531 (2008).
- [32] S. Kuroyanagi, T. Chiba, and N. Sugiyama, Precision calculations of the gravitational wave background spectrum from inflation, Phys. Rev. D **79**, 103501 (2009).
- [33] K. Nakayama and J. Yokoyama, Gravitational wave background and non-gaussianity as a probe of the curvaton scenario, J. Cosmol. Astropart. Phys. 01 (2010) 010.
- [34] S. Kuroyanagi, C. Ringeval, and T. Takahashi, Early universe tomography with CMB and gravitational waves, Phys. Rev. D 87, 083502 (2013).
- [35] R. Jinno, T. Moroi, and K. Nakayama, Inflationary gravitational waves and the evolution of the early universe, J. Cosmol. Astropart. Phys. 01 (2014) 040.
- [36] K. Saikawa and S. Shirai, Primordial gravitational waves, precisely: The role of thermodynamics in the standard model, J. Cosmol. Astropart. Phys. 05 (2018) 035.
- [37] C. Chen, K. Dimopoulos, C. Eröncel, and A. Ghoshal, Enhanced primordial gravitational waves from a stiff post-inflationary era due to an oscillating inflaton, Phys. Rev. D **110**, 063554 (2024).
- [38] K. Nakayama, S. Saito, Y. Suwa, and J. Yokoyama, Space laser interferometers can determine the thermal history of the early Universe, Phys. Rev. D 77, 124001 (2008).
- [39] K. Nakayama, S. Saito, Y. Suwa, and J. Yokoyama, Probing reheating temperature of the universe with gravitational wave background, J. Cosmol. Astropart. Phys. 06 (2008) 020.

- [40] S. Kuroyanagi, K. Nakayama, and S. Saito, Prospects for determination of thermal history after inflation with future gravitational wave detectors, Phys. Rev. D 84, 123513 (2011).
- [41] W. Buchmüller, V. Domcke, K. Kamada, and K. Schmitz, The gravitational wave spectrum from cosmological B-L breaking, J. Cosmol. Astropart. Phys. 10 (2013) 003.
- [42] W. Buchmuller, V. Domcke, K. Kamada, and K. Schmitz, A minimal supersymmetric model of particle physics and the early universe, arXiv:1309.7788.
- [43] R. Jinno, T. Moroi, and T. Takahashi, Studying inflation with future space-based gravitational wave detectors, J. Cosmol. Astropart. Phys. 12 (2014) 006.
- [44] S. Kuroyanagi, K. Nakayama, and J. Yokoyama, Prospects of determination of reheating temperature after inflation by DECIGO, Prog. Theor. Exp. Phys. 2015, 013E02 (2015).
- [45] N. Bernal, A. Ghoshal, F. Hajkarim, and G. Lambiase, Primordial gravitational wave signals in modified cosmologies, J. Cosmol. Astropart. Phys. 11 (2020) 051.
- [46] A. Ghoshal, Y. Gouttenoire, L. Heurtier, and P. Simakachorn, Primordial black hole archaeology with gravitational waves from cosmic strings, J. High Energy Phys. 08 (2023) 196.
- [47] A. Ghoshal, L. Heurtier, and A. Paul, Signatures of nonthermal dark matter with kination and early matter domination. Gravitational waves versus laboratory searches, J. High Energy Phys. 12 (2022) 105.
- [48] M. Berbig and A. Ghoshal, Impact of high-scale seesaw and leptogenesis on inflationary tensor perturbations as detectable gravitational waves, J. High Energy Phys. 05 (2023) 172.
- [49] Z. A. Borboruah, A. Ghoshal, L. Malhotra, and U. Yajnik, Inflationary gravitational wave spectral shapes as test for low-scale leptogenesis, arXiv:2405.06603.
- [50] Z. A. Borboruah, A. Ghoshal, and S. Ipek, Probing flavor violation and baryogenesis via primordial gravitational waves, J. High Energy Phys. 07 (2024) 228.
- [51] A. Ghoshal, D. Paul, and S. Pal, Primordial gravitational waves as probe of dark matter in interferometer missions: Fisher forecast and MCMC, J. High Energy Phys. 12 (2024) 150.
- [52] S. Datta and R. Samanta, Gravitational waves-tomography of low-scale-leptogenesis, J. High Energy Phys. 11 (2022) 159.
- [53] S. Datta and R. Samanta, Fingerprints of GeV scale right-handed neutrinos on inflationary gravitational waves and PTA data, Phys. Rev. D 108, L091706 (2023).
- [54] M. Chianese, S. Datta, R. Samanta, and N. Saviano, Tomography of flavoured leptogenesis with primordial blue gravitational waves, J. Cosmol. Astropart. Phys. 11 (2024) 051.
- [55] S. Datta, A. Ghosal, A. Ghoshal, and G. White, Complementarity between cosmic string gravitational waves and long lived particle searches in laboratory, Phys. Rev. D 112, 015009 (2025).
- [56] J. L. Feng *et al.*, The forward physics facility at the high-luminosity LHC, J. Phys. G **50**, 030501 (2023).
- [57] R. Acciarri *et al.* (DUNE Collaboration), Long-baseline neutrino facility (LBNF) and deep underground neutrino experiment (DUNE): Conceptual design report, volume 2:

- The physics program for DUNE at LBNF, arXiv:1512 .06148.
- [58] J. M. Berryman, A. de Gouvea, P. J. Fox, B. J. Kayser, K. J. Kelly, and J. L. Raaf, Searches for decays of new particles in the DUNE multi-purpose near detector, J. High Energy Phys. 02 (2020) 174.
- [59] D. Curtin *et al.*, Long-lived particles at the energy frontier: The MATHUSLA physics case, Rep. Prog. Phys. 82, 116201 (2019).
- [60] D. Curtin and J. S. Grewal, Long lived particle decays in MATHUSLA, Phys. Rev. D 109, 075017 (2024).
- [61] M. Anelli et al. (SHiP Collaboration), A facility to search for hidden particles (SHiP) at the CERN SPS, arXiv:1504.04956.
- [62] M. Aker *et al.* (Katrin Collaboration), Direct neutrino-mass measurement based on 259 days of KATRIN data, Science 388, adq9592 (2025).
- [63] I. Esteban, M. C. Gonzalez-Garcia, M. Maltoni, T. Schwetz, and A. Zhou, The fate of hints: Updated global analysis of three-flavor neutrino oscillations, J. High Energy Phys. 09 (2020) 178.
- [64] J. L. Feng, A. Hewitt, F. Kling, and D. La Rocco, Simulating heavy neutral leptons with general couplings at collider and fixed target experiments, Phys. Rev. D 110, 035029 (2024).
- [65] B. Barman, P. S. Bhupal Dev, and A. Ghoshal, Probing freeze-in dark matter via heavy neutrino portal, Phys. Rev. D 108, 035037 (2023).
- [66] M. Agostini, G. Benato, J. A. Detwiler, J. Menéndez, and F. Vissani, Toward the discovery of matter creation with neutrinoless double-beta decay, Rev. Mod. Phys. 95, 025002 (2023).
- [67] M. Doi *et al.*, Neutrino mass, the right-handed interaction and the double beta decay. I: Formalism, Phys. Theor. Phys. **66**, 1739 (1983).
- [68] V. Cirigliano, W. Dekens, J. de Vries, M. Graesser, and E. Mereghetti, Neutrinoless double beta decay in chiral effective field theory: Lepton number violation at dimension seven, J. High Energy Phys. 12 (2017) 082.
- [69] L. Graf, F. F. Deppisch, F. Iachello, and J. Kotila, Short-range neutrinoless double beta decay mechanisms, Phys. Rev. D 98, 095023 (2018).
- [70] F. F. Deppisch, L. Graf, F. Iachello, and J. Kotila, Analysis of light neutrino exchange and short-range mechanisms in $0\nu\beta\beta$ decay, Phys. Rev. D **102**, 095016 (2020).
- [71] F. F. Deppisch, K. Fridell, and J. Harz, Constraining lepton number violating interactions in rare kaon decays, J. High Energy Phys. 12 (2020) 186.
- [72] P. D. Bolton, F. F. Deppisch, L. Gráf, and F. Šimkovic, Two-neutrino double beta decay with sterile neutrinos, Phys. Rev. D 103, 055019 (2021).
- [73] P. D. Bolton, F. F. Deppisch, K. Fridell, J. Harz, C. Hati, and S. Kulkarni, Probing active-sterile neutrino transition magnetic moments with photon emission from CEνNS, Phys. Rev. D 106, 035036 (2022).
- [74] M. Agostini, F. F. Deppisch, and G. Van Goffrier, Probing the mechanism of neutrinoless double-beta decay in multiple isotopes, J. High Energy Phys. 02 (2023) 172.
- [75] P. D. Bolton, F. F. Deppisch, and P. S. B. Dev, Probes of heavy sterile neutrinos, in *56th Rencontres de Moriond on*

- Electroweak Interactions and Unified Theories (2022), arXiv:2206.01140.
- [76] A. Babič, S. Kovalenko, M. I. Krivoruchenko, and F. Šimkovic, Interpolating formula for the $0\nu\beta\beta$ -decay half-life in the case of light and heavy neutrino mass mechanisms, Phys. Rev. D **98**, 015003 (2018).
- [77] W. Dekens, J. de Vries, K. Fuyuto, E. Mereghetti, and G. Zhou, Sterile neutrinos and neutrinoless double beta decay in effective field theory, J. High Energy Phys. 06 (2020) 007
- [78] A. J. Zsigmond (LEGEND Collaboration), LEGEND: The future of neutrinoless double-beta decay search with germanium detectors, J. Phys. Conf. Ser. 1468, 012111 (2020).
- [79] A. Gando *et al.* (KamLAND-Zen Collaboration Collaboration), Search for Majorana neutrinos near the inverted mass hierarchy region with KamLAND-Zen, Phys. Rev. Lett. 117, 082503 (2016).
- [80] M. Agostini *et al.* (GERDA Collaboration), Final results of GERDA on the search for neutrinoless double-β decay, Phys. Rev. Lett. **125**, 252502 (2020).
- [81] A. Boyarsky, M. Ovchynnikov, O. Ruchayskiy, and V. Syvolap, Improved big bang nucleosynthesis constraints on heavy neutral leptons, Phys. Rev. D 104, 023517 (2021).
- [82] N. Sabti, A. Magalich, and A. Filimonova, An extended analysis of heavy neutral leptons during big bang nucleosynthesis, J. Cosmol. Astropart. Phys. 11 (2020) 056.
- [83] V. Syvolap, Astrophysical and cosmological constraints on parameters of hypothetical particles, Ph.D. thesis, Københavns Universitet, Faculty of Science, Niels Bohr Institute, Københavns Universitet, Faculty of Science, SCIENCE Faculty Office, Bohr Inst., 2021.
- [84] D. Nötzold and G. Raffelt, Neutrino dispersion at finite temperature and density, Nucl. Phys. B307, 924 (1988).
- [85] A. D. Dolgov and S. H. Hansen, Massive sterile neutrinos as warm dark matter, Astropart. Phys. 16, 339 (2002).
- [86] A. Boyarsky, O. Ruchayskiy, and M. Shaposhnikov, The role of sterile neutrinos in cosmology and astrophysics, Annu. Rev. Nucl. Part. Sci. **59**, 191 (2009).
- [87] S. Dodelson and L. M. Widrow, Sterile-neutrinos as dark matter, Phys. Rev. Lett. 72, 17 (1994).
- [88] R. Barbieri and A. Dolgov, Bounds on sterile-neutrinos from nucleosynthesis, Phys. Lett. B 237, 440 (1990).
- [89] G. F. Giudice, M. Peloso, A. Riotto, and I. Tkachev, Production of massive fermions at preheating and leptogenesis, J. High Energy Phys. 08 (1999) 014.
- [90] R. J. Scherrer and M. S. Turner, Decaying particles do not heat up the universe, Phys. Rev. D **31**, 681 (1985).
- [91] F. Bezrukov, H. Hettmansperger, and M. Lindner, keV sterile neutrino Dark Matter in gauge extensions of the Standard Model, Phys. Rev. D 81, 085032 (2010).
- [92] Y. Akrami *et al.* (Planck Collaboration), Planck 2018 results. X. Constraints on inflation, Astron. Astrophys. **641**, A10 (2020).
- [93] P. A. R. Ade *et al.* (BICEP and Keck Collaborations), Improved constraints on primordial gravitational waves using Planck, WMAP, and BICEP/Keck observations through the 2018 observing season, Phys. Rev. Lett. 127, 151301 (2021).

- [94] A. R. Liddle and D. H. Lyth, The cold dark matter density perturbation, Phys. Rep. 231, 1 (1993).
- [95] R. H. Brandenberger, A. Nayeri, S. P. Patil, and C. Vafa, Tensor modes from a primordial hagedorn phase of string cosmology, Phys. Rev. Lett. 98, 231302 (2007).
- [96] M. Baldi, F. Finelli, and S. Matarrese, Inflation with violation of the null energy condition, Phys. Rev. D 72, 083504 (2005).
- [97] T. Kobayashi, M. Yamaguchi, and J. Yokoyama, G-inflation: Inflation driven by the Galileon field, Phys. Rev. Lett. 105, 231302 (2010).
- [98] G. Calcagni and S. Tsujikawa, Observational constraints on patch inflation in noncommutative spacetime, Phys. Rev. D 70, 103514 (2004).
- [99] G. Calcagni, S. Kuroyanagi, J. Ohashi, and S. Tsujikawa, Strong Planck constraints on braneworld and non-commutative inflation, J. Cosmol. Astropart. Phys. 03 (2014) 052.
- [100] J. L. Cook and L. Sorbo, Particle production during inflation and gravitational waves detectable by groundbased interferometers, Phys. Rev. D 85, 023534 (2012).
- [101] S. Mukohyama, R. Namba, M. Peloso, and G. Shiu, Blue tensor spectrum from particle production during inflation, J. Cosmol. Astropart. Phys. 08 (2014) 036.
- [102] S. Kuroyanagi, T. Takahashi, and S. Yokoyama, Blue-tilted inflationary tensor spectrum and reheating in the light of NANOGrav results, J. Cosmol. Astropart. Phys. 01 (2021) 071.
- [103] S. Kuroyanagi, T. Takahashi, and S. Yokoyama, Blue-tilted tensor spectrum and thermal history of the universe, J. Cosmol. Astropart. Phys. 02 (2015) 003.
- [104] J. Aasi et al. (LIGO Scientific Collaboration), Advanced LIGO, Classical Quantum Gravity 32, 074001 (2015).
- [105] K. Yagi and N. Seto, Detector configuration of DECIGO/BBO and identification of cosmological neutron-star binaries, Phys. Rev. D 83, 044011 (2011).
- [106] P. Amaro-Seoane *et al.*, Laser interferometer space antenna, arXiv:1702.00786.
- [107] M. Punturo *et al.* (ET Collaboration), The Einstein telescope: A third-generation gravitational wave observatory, Classical Quantum Gravity **27**, 194002 (2010).
- [108] J. Garcia-Bellido, H. Murayama, and G. White, Exploring the early Universe with Gaia and Theia, J. Cosmol. Astropart. Phys. 12 (2021) 023.
- [109] A. Sesana *et al.*, Unveiling the gravitational universe at μ -Hz frequencies, Exp. Astron. **51**, 1333 (2021).
- [110] J. Antoniadis *et al.*, The second data release from the European Pulsar Timing Array III. Search for gravitational wave signals, Astron. Astrophys. **678**, A50 (2023).
- [111] A. Kogut *et al.*, The primordial inflation explorer (PIXIE): Mission design and science goals, J. Cosmol. Astropart. Phys. 04 (2025) 020.
- [112] K. Basu *et al.*, A space mission to map the entire observable universe using the CMB as a backlight: Voyage 2050 science white paper, Exp. Astron. **51**, 1555 (2021).
- [113] T.-H. Yeh, K. A. Olive, and B. D. Fields, Limits on non-relativistic matter during Big-bang nucleosynthesis, J. Cosmol. Astropart. Phys. 07 (2024) 016.
- [114] Y.-M. Chen and Y. Zhang, BBN constraint on heavy neutrino production and decay, Phys. Rev. D 111, 123024 (2025).

- [115] C. Caprini and D. G. Figueroa, Cosmological backgrounds of gravitational waves, Classical Quantum Gravity 35, 163001 (2018).
- [116] M. Breitbach, J. Kopp, E. Madge, T. Opferkuch, and P. Schwaller, Dark, cold, and noisy: Constraining secluded hidden sectors with gravitational waves, J. Cosmol. Astropart. Phys. 07 (2019) 007.
- [117] M. Maggiore, Gravitational wave experiments and early universe cosmology, Phys. Rep. 331, 283 (2000).
- [118] N. Aghanim *et al.* (Planck Collaboration), Planck 2018 results. VI. Cosmological parameters, Astron. Astrophys. **641**, A6 (2020); Astron. Astrophys. **652**, C4(E) (2021).
- [119] K. Abazajian *et al.* (CMB-S4 Collaboration), CMB-S4: Forecasting constraints on primordial gravitational waves, Astrophys. J. **926**, 54 (2022).
- [120] K. Abazajian *et al.* (CMB-S4 Collaboration), Snowmass 2021 CMB-S4 white paper, arXiv:2203.08024.
- [121] C.-B. A. I. C. Consortium (CMB-Bharat Collaboration), Exploring cosmic history and origin: A proposal for a next generation space mission for near-ultimate measurements of the Cosmic Microwave Background (CMB) polarization and discovery of global CMB spectral distortions, https:// cmb-bharat.in/wp-content/uploads/2018/06/cmb-bharatrao-tp-es.pdf.
- [122] N. Sehgal et al., CMB-HD: An ultra-deep, high-resolution millimeter-wave survey over half the sky, Bull. Am. Astron. Soc. 51, 1 (2019), https://inspirehep.net/literature/ 1741243.
- [123] S. Aiola *et al.* (CMB-HD Collaboration), Snow-mass2021 CMB-HD white paper, arXiv:2203.05728.

- [124] A. Dasgupta, P. S. B. Dev, A. Ghoshal, and A. Mazumdar, Gravitational wave pathway to testable leptogenesis, Phys. Rev. D 106, 075027 (2022).
- [125] N. Bhaumik, A. Ghoshal, and M. Lewicki, Doubly peaked induced stochastic gravitational wave background: Testing baryogenesis from primordial black holes, J. High Energy Phys. 07 (2022) 130.
- [126] B. Barman, D. Borah, A. Dasgupta, and A. Ghoshal, Probing high scale Dirac leptogenesis via gravitational waves from domain walls, Phys. Rev. D 106, 015007 (2022).
- [127] A. Ghoshal and P. Saha, Detectable gravitational waves from preheating probes nonthermal dark matter, Phys. Rev. D 109, 023526 (2024).
- [128] D. I. Dunsky, A. Ghoshal, H. Murayama, Y. Sakakihara, and G. White, GUTs, hybrid topological defects, and gravitational waves, Phys. Rev. D 106, 075030 (2022).
- [129] A. Ghoshal and A. Salvio, Gravitational waves from fundamental axion dynamics, J. High Energy Phys. 12 (2020) 049.
- [130] P. D. Bolton, F. F. Deppisch, M. Rai, and Z. Zhang, Probing the nature of heavy neutral leptons in direct searches and neutrinoless double beta decay, Nucl. Phys. B1010, 116785 (2025).
- [131] F. F. Deppisch, T. E. Gonzalo, C. Majumdar, and Z. Zhang, Relaxing limits from big bang nucleosynthesis on heavy neutral leptons with axion-like particles, J. Cosmol. Astropart. Phys. 02 (2025) 054.
- [132] J. Klarić, M. Shaposhnikov, and I. Timiryasov, Uniting low-scale leptogenesis mechanisms, Phys. Rev. Lett. 127, 111802 (2021).